Two Structural Transitions in Membrane Pore Formation by Pneumolysin, the Pore-Forming Toxin of *Streptococcus pneumoniae*

Robert J. C. Gilbert,*# Jose L. Jiménez,[†]
Shaoxia Chen,[†] Ian J. Tickle,[†]
Jamie Rossjohn,[‡] Michael Parker,[‡]
Peter W. Andrew,[§] and Helen R. Saibil[†‖]
*Department of Biochemistry
University of Leicester
Leicester LE1 7RH
United Kingdom
[†]Department of Crystallography
Birkbeck College
Malet Street
London WC1E 7HX
United Kingdom
[‡]St. Vincent's Institute of Medical Research
41 Victoria Parade
Fitzroy, Victoria 3065
Australia
[§]Department of Microbiology and Immunology
University of Leicester
Leicester LE1 8AH
United Kingdom

Summary

The human pathogen *Streptococcus pneumoniae* produces soluble pneumolysin monomers that bind host cell membranes to form ring-shaped, oligomeric pores. We have determined three-dimensional structures of a helical oligomer of pneumolysin and of a membrane-bound ring form by cryo-electron microscopy. Fitting the four domains from the crystal structure of the closely related perfringolysin reveals major domain rotations during pore assembly. Oligomerization results in the expulsion of domain 3 from its original position in the monomer. However, domain 3 reassociates with the other domains in the membrane pore form. The base of domain 4 contacts the bilayer, possibly along with an extension of domain 3. These results reveal a two-stage mechanism for pore formation by the cholesterol-binding toxins.

Introduction

Pneumolysin is an important virulence factor of the human pathogen *Streptococcus pneumoniae* (the pneumococcus). The pneumococcus causes pneumonia, meningitis, and otitis media (Alonso de Velasco et al., 1995). In pneumococcal strains incapable of producing pneumolysin, the bacterial virulence is heavily attenuated (Berry et al., 1989). The action of pneumolysin occurs according to two main mechanisms: damage to cell membranes by pore formation, and activation of the complement system in a nonimmunospecific manner through

‖To whom correspondence should be addressed (e-mail: h.saibil@mail.cryst.bbk.ac.uk).
#Present address: Laboratory of Molecular Biophysics, University of Oxford, Oxford OX1 3QU, United Kingdom.

direct interaction with the IgG domain Fc (Mitchell et al., 1991). These activities together are thought to underpin the mechanisms of inflammation and membrane damage associated with pneumolysin in pneumococcal disease (Alexander et al., 1998).

Pneumolysin is a member of a large family of highly homologous bacterial protein toxins (Tweten, 1995; Morgan et al., 1996). We refer to them as cholesterol-binding toxins, a more appropriate name than the original "thiol-activated toxins," which arose from the observation that modification of a conserved cysteine causes inactivation. Members of the family occur in four Gram-positive genera, *Streptococcus*, *Clostridium*, *Listeria*, and *Bacillus*, and include perfringolysin from *C. perfringens* and streptolysin from *S. pyogenes*, as well as pneumolysin. The crystal structure of perfringolysin has been determined in its soluble, monomeric form (Figure 1) (Rossjohn et al., 1997). Perfringolysin shares 48% sequence identity and 60% sequence similarity with pneumolysin, so it is clear that they are structurally and functionally homologous. The four domains of the monomeric form, consisting predominantly of β sheet structure, pack into a planar, elongated shape of 110 × 55 × 30 Å. The most conserved region in the cholesterol-binding toxins is an 11-residue sequence containing three tryptophans (the Trp-rich loop) at the base of domain 4. The Trp-rich loop is associated with membrane binding by these toxins. Sites of mutations affecting oligomerization, pore formation, and complement activation are also shown in Figure 1.

The pore-forming activity of pneumolysin is associated with binding of cholesterol in cell membranes (Watson et al., 1972). Cholesterol-mediated binding to the membrane occurs through domain 4 of pneumolysin and is thought to involve the extension and insertion of the Trp-rich loop in the form of a hydrophobic dagger (Rossjohn et al., 1997; Nakamura et al., 1998). In addition, cysteine scanning mutagenesis combined with fluorescence spectroscopy studies of streptolysin and perfringolysin have implicated part of domain 3 in membrane insertion (Palmer et al., 1996; Shepard et al., 1998). An α-helical region (residues 158–187 in pneumolysin; 189–218 in perfringolysin), which is buried in the interior of the monomer structure, is proposed to adopt a β hairpin structure in the pore (Shepard et al., 1998). The formation of pores following membrane binding is associated with the assembly of toxin into rings of 30–50 subunits (Olofsson et al., 1993; Sekiya et al., 1993; Morgan et al., 1995). The rings are 350–450 Å in diameter and can create extremely large pores that are permeable to proteins. This property of cholesterol-binding toxins has been exploited (notably with streptolysin) in their use for the exchange of macromolecules in the cytosol (e.g., Grindstaff et al., 1998). However, the oligomers also occur in incomplete arc-shaped forms (Bhakdi et al., 1985; Morgan et al., 1994). There is strong evidence that these arcs and even smaller aggregates of streptolysin can form conducting pores (Palmer et al., 1995, 1998), which appears to rule out the simple idea that the ring forms a giant β barrel. Negative-stain electron
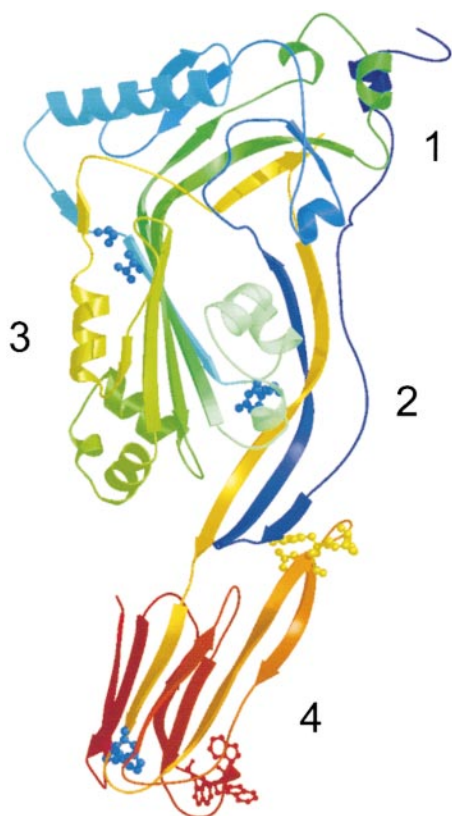
Figure 1. The Soluble, Monomeric Form of Perfringolysin

A ribbon representation of the α-carbon backbone is colored by sequence with the four domains numbered. The Trp-rich loop involved in membrane binding is at the bottom right. The three small helices (light green) in domain 3, adjacent to domain 2, have been proposed to refold to a β hairpin structure and enter the membrane during pore formation (Shepard et al., 1998). Residues whose mutation or chemical modification interferes with function (Rossjohn et al., 1998) are shown in ball-and-stick representation: blue, pore formation; red, membrane/cholesterol binding; yellow, complement activation.

microscopy (EM) of the rings and helical stacks suggested that the four domains are packed in a square-planar arrangement, with the planes stacked up around the rings (Morgan et al., 1995).

Pneumolysin can polymerize in solution in the absence of cholesterol or cholesterol-containing membranes (Gilbert et al., 1998). The resulting assemblies appear the same as isolated oligomers that have been formed in the presence of membranes (Morgan et al., 1995). At high protein concentration the rings are accompanied by helical oligomers with a similar subunit conformation. We have used the helical form of pneumolysin to obtain a three-dimensional (3D) reconstruction of this oligomeric form using cryo-electron microscopy (cryo-EM) and a combination of helical and single-particle analysis. This has revealed an unexpected domain arrangement in the isolated oligomer, in which domain 3 is extruded from its original position in the monomer and becomes disordered. We have also obtained tangential views of pores bound to small liposomes. The density in the ring profiles shows that during pore formation the domains rearrange into a third conformation

with a thin stalk extending down from the base of the ring into the membrane bilayer. Domain 3 repacks against the other domains, but its transient extrusion could allow the α-helical region originally buried inside the monomer to extend down into the membrane along with the base of domain 4. We describe a model for pore formation based on these results.

Results

Cryo-EM of Pneumolysin Helices
We chose the helical form of pneumolysin for 3D reconstruction, since the helices present all the necessary views, unlike the isolated ring form, which is only observed in end view on EM grids. Although the helical oligomer would not occur physiologically, the end views of helices and isolated rings, formed either in the presence or absence of membranes, show that the major features of subunit conformation are the same in the two forms. The main difficulty was that the helices are not very well ordered. Helix images were interpolated to a straight axis, and then diffraction patterns were calculated to assess the packing and degree of order. A raw image and the corresponding diffraction pattern of one such helix are shown in Figures 2a and 2b. Some details of the subunit structure are evident in the raw images. The short helix seen in end view shows the characteristic concentric rings, and the side views provided by the longer helices also show two layers of density in the side projection, with an opening in the middle of each subunit. These views confirm the conclusions from earlier negative-stain EM work (Morgan et al., 1995), in particular regarding the side view, which is much more distinct in the cryo-EM images.

The helices showed variations in pitch that limited the number of visible layer lines. We therefore adopted a single-particle strategy (Jiménez et al., 1999) and cut the digitized, straightened helices into single pitch repeats. These cut-out repeats were aligned and averaged as single particles. This method produced a greatly improved image of the pitch repeat, which was then used to generate a helical reconstruction. From the negative-stain study (Morgan et al., 1995), we knew that the number of subunits per ring was in the range 40–50. From the diameter of the helical form, we estimated 41 subunits per turn. This value gave a good fit to the input data, but the intersubunit distance is close to the resolution limit of the data, so subunit repeats over a range around 41 are also possible. The reprojected view of this reconstruction and the corresponding diffraction pattern are shown in Figures 2c and 2d. The original features are present, but the resolution is greatly improved, with information extending to ~25 Å on the diffraction pattern.

3D Structure of the Helical Oligomer
A surface-rendered representation of the 3D reconstruction of the pneumolysin oligomer is shown in Figure 3a. Although the individual subunits are not quite separately resolved, the polarity and subunit shape are distinct, with a prominent ridge on the outside of the oligomer and the opening in the subunit facing the interior. To check the consistency of the reconstruction, the end
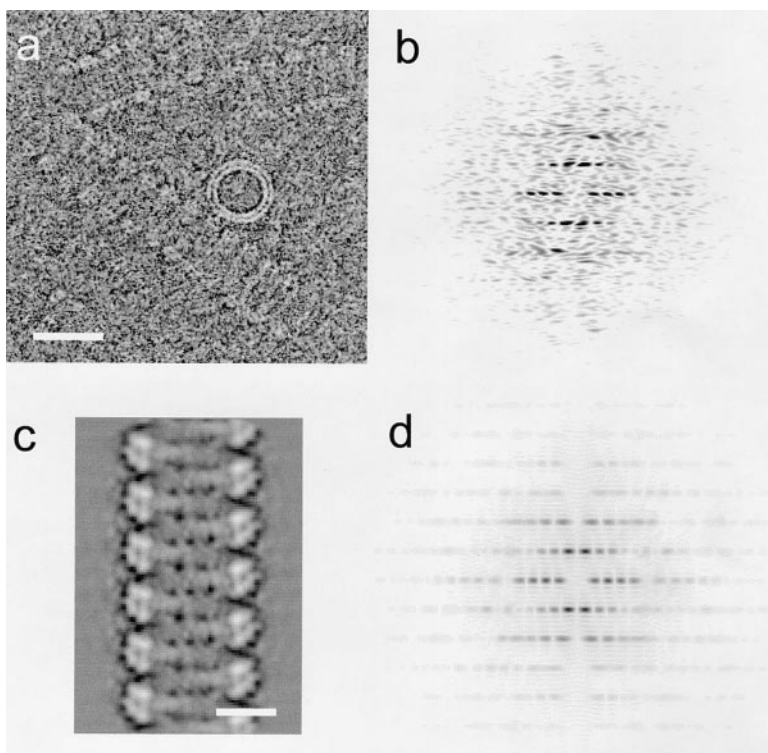
Figure 2. Cryo-EM of the Helical, Oligomeric Form of Pneumolysin

(a) Cryo-electron micrograph of pneumolysin oligomers, showing helices in side view and a short helix in end view. The two concentric rings of density are particularly clear in the helix end view. End views of arcs and rings are also present but have very weak contrast.
(b) Computed diffraction pattern of the long helix after straightening. The layer line repeat is 135 Å.
(c) Reprojection of a 3D reconstruction of the helical form. The two-layered projection of the subunit structure is evident at the edges of the helix, as is the polarity of the structure.
(d) Diffraction pattern of (c). The strong features correspond to those in (b), but the resolution is much improved.
Scale bars: (a), 350 Å; (c), 150 Å.

projection of the map (Figure 3c) is compared to the symmetry-averaged view of a ring with 41-fold symmetry from the earlier negative-stain EM study (Figure 3d). Although some of the subunit repeat features are smoothed out in the cryo-EM reprojection, the two concentric layers of density are present. The end view projections (Figures 3c and 3d) and the subunit dimensions require the planar subunits to be vertically oriented in the helix, perhaps at a slight angle to the radial direction. Therefore, the subunit shape is revealed by the axial section through the helix density (Figure 3b). The bent conformation of the monomer, with a central cavity, is dramatically different from the rectangular, soluble monomer structure determined by X-ray crystallography (Figure 1; Rossjohn et al., 1997).

Fitting the Domain Atomic Structures into the Oligomer Density Map

The four domains of the perfringolysin atomic structure were separated at the boundaries determined by Rossjohn et al. (1997) in order to fit them into the EM density as rigid bodies with interdomain hinge rotations. The major changes are that domain 4 must rotate up by 45° relative to domain 2 to fit into the density and domain 3 is mostly absent from the EM density (Figure 4a). A conserved glycine residue in the region of extended chain between domains 2 and 4 is compatible with the large rotation of domain 4. The fit for domains 1, 2, and 4 is reasonable. It might be improved by bending domain 2, which is long and thin with high temperature factors, but such an alteration would not be justified on the basis of the low-resolution density. The large rotation of domain 4 is incompatible with the original position

of domain 3, which must be pushed out of its pocket between the other domains. Its absence from the averaged EM density indicates that it occupies multiple positions and/or conformations. The fit shows that the oligomer structure is completely different from that in previous proposals, in which the opposite side of the molecule faced the pore, which would have been lined by domain 2 (Bayley, 1997; Rossjohn et al., 1997, 1998). The structure with domain 3 in an expelled position is shown in Figure 4b.

The polarity of the structure guided the overall orientation of the fit. Domain 1 is too large and the wrong shape to fit into the smaller lobe of density. Moreover, domain 4 would only fill a small part of the larger lobe, which can easily be filled by domain 1 plus the adjacent part of domain 3.

In order to assess the validity of the fit, a projected density map was created from the fitted domains and filtered to low resolution in order to compare it with the image data. Figure 4c shows a side view sliced out of the 3D map, compared to the side view of the fitted monomer (Figure 4d). The overall features are similar, apart from some residual domain 3 density bridging between the ends of domains 1 and 4, supporting the fitted domain 1, 2, and 4 arrangement. Cross correlations of model densities with the map section were calculated for various 180° rotations of the model (left-right or top-bottom). Rotations from the chosen fit caused 12%–22% reductions in the correlation coefficient, supporting the chosen orientation. The end projection (data not shown) of a partial oligomer model (Figure 7d) also shows two concentric layers of density, supporting the general features of the fitted structure. Domains 1 and 4 provide the subunit contacts forming the oligomer.
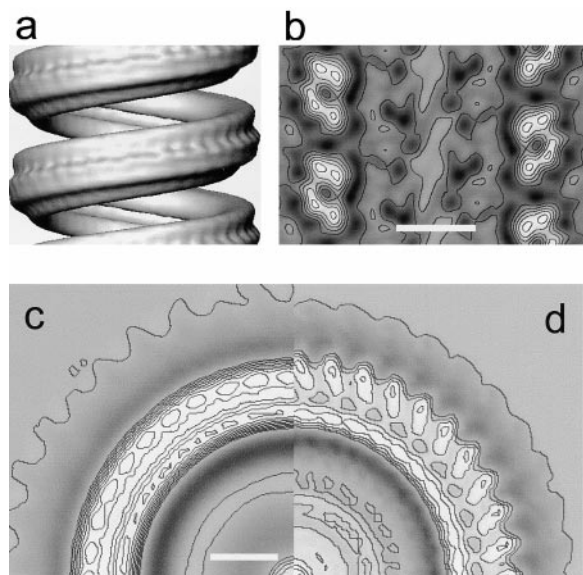
Figure 3. 3D Structure and End Projections of the Helical Oligomer

(a) Surface-rendered view of the 3D reconstruction of the pneumo-lysin helical oligomer with 41 subunits per turn.

(b) Contoured density of a central slice through the 3D map, showing the subunit shape.

(c) Projection of the 3D map along the helix axis, showing the two concentric rings of density.

(d) Symmetry-averaged view of a pneumolysin ring from the nega-tive-stain EM study of Morgan et al (1995), scaled to match (c). In this case the symmetry was shown to be 41-fold by rotational correlation analysis. The subunit projections are better resolved in the negatively stained image.

Scale bars: (b), 100 Å; (c), 50 Å.

The Membrane-Bound Oligomer

Cryo-EM images of liposomes with bound pneumolysin (Figure 5a) yielded tangential views containing membrane-bound rings seen edge-on (side views), and barely discernable ring images (end views). We refer to them as pores, since they are formed on liposomes with a similar sterol and lipid composition as red blood cell membranes, under conditions that produce conducting pores in planar lipid films. Suitable liposomes had to be small enough to avoid flattening in the vitrified ice layer but large enough to bind pores. The edges of the pores seen in side view projection are prominent, resembling spikes protruding from the membrane surface. A faint bar of density outside the membrane joins the prominent edge features. A set of 97 side views of apparently com-plete pores were aligned and sorted by multivariate sta-tistical analysis into classes. The largest class contained 26 images whose average (Figure 5b) reveals the oligo-meric ring structure perched ~25 Å above the bilayer surface, with narrow extensions of the base bridging the gap. The class average was used to generate a 3D reconstruction of the ring, using the 33-fold symmetry estimated from the ring diameter. The reprojection of this 3D reconstruction (Figure 5c) matches well with the input image (Figure 5b). A slice through the 3D map (Figure 5d) shows that the oligomer lies almost com-pletely outside the bilayer, resembling a crown on the membrane surface as noted by Sekiya et al. (1993). Re-markably, the ring profile shows yet a third conformation

of the pneumolysin subunit. Instead of the cavity left by the extrusion of domain 3 from the helical oligomer, there is an inward protrusion of density. In fact, the whole curvature of the subunit seems to have been re-versed, with the outside now curved inward. Curiously, the membrane appears to be continuous inside the pore, but there are fluctuations in its density that might indi-cate the presence of nonbilayer lipid phases. The region of lowest density in the membrane is just outside the pore subunits. The membrane-bound reconstruction had a resolution determined by Fourier ring correlation of ~33 Å.

As before, we fitted the perfringolysin domains into the profile of the reconstruction. The density envelope and fit are shown in Figure 6a. Almost the whole toxin molecule resides outside the bilayer. Domain 4 may be partially inserted into the membrane (Nakamura et al., 1995, 1998), particularly if the Trp-rich motif is extended as previously proposed (Rossjohn et al., 1997). The do-main orientations are roughly similar to those in the monomer, but domain 3 packs more tightly against do-main 2, altering its angle with domain 1. We excluded the three small helices at the interface between domains 3 and 2 because two separate lines of enquiry have implicated this region in a structural transition and mem-brane insertion during pore formation (Palmer et al., 1996; Shepard et al., 1998). We compared the low-reso-lution density map created from the model (Figure 6b) to the observed profile in Figure 6c. Again, the chosen orientation of the molecule provides a better fit than 180° rotated alternatives, which gave a 13%–22% drop in correlation coefficient. The fit of domain 4 might be improved by slightly twisting it out of the plane, but the resolution of our map was not sufficient to assess out of plane movements. An oligomeric model of the pore (Figure 7e) also shows that the packing between the fourth domains could accommodate a thin extension of domain 3. End projections of the subunit with all four domains present give rise to a single, diffuse ring, rather than the concentric rings of the helical or isolated ring form.

Discussion

The oligomerization of the cholesterol-binding toxins into ring-shaped, membrane-bound structures is funda-mental to the mechanism by which they damage mem-branes and cause cell lysis (Harris et al., 1991; Palmer et al., 1998). Oligomerization into arcs, rings, and helices can occur in solution (Gilbert et al., 1998), and we have used a helical form to determine the initial conforma-tional changes that accompany oligomerization. Side views of oligomeric rings bound to liposomes have been used to define the conformation of the pore state.

Conformation of the Isolated Oligomer:
An Intermediate in Pore Formation

The rings and helices that form at high toxin concentra-tion in the absence of cholesterol-containing mem-branes have a distinctive double concentric ring appear-ance, due to the expulsion of domain 3 and the formation of an internal cavity in each subunit. The same double
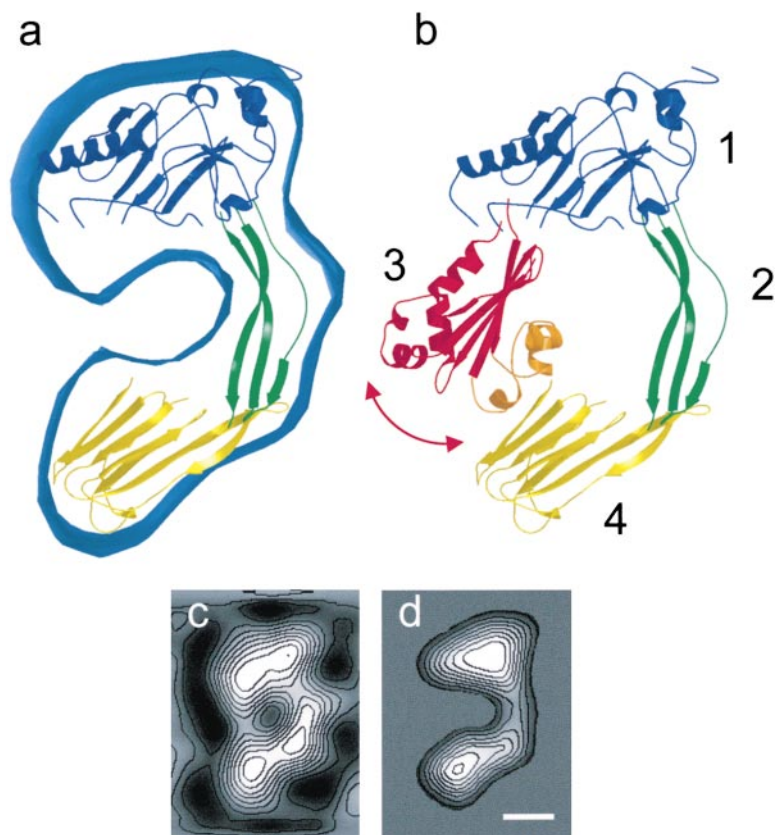
Figure 4. Fitting the Atomic Structure of the Perfringolysin Domains into the Helical Density Map

(a) Fit of domains 1, 2, and 4. The upward movement of domain 4 excludes domain 3 from its original position. There is little density in the EM map for domain 3.

(b) View showing an arbitrarily chosen position that domain 3 could adopt after swinging out of the cavity. Unfolding of the helical region (orange) could allow the rest of domain 3 to adopt a more vertical orientation, corresponding to the bridge of weak density between the ends of domains 1 and 4 in (c). Blue, domain 1; green, domain 2; red, domain 3; orange, domain 3 helical region thought to insert into the membrane; yellow, domain 4.

(c) Slice of the map showing the density profile of a subunit.

(d) Reprojection of the fitted model for domains 1, 2, and 4 filtered to 24 Å resolution. Scale bar for (c) and (d), 30 Å.

ring profile is seen in isolated rings formed in the presence of membranes (Morgan et al., 1995; cryo-EM data not shown). The expulsion of domain 3 accompanies the rotation of domain 4 into its position in the oligomer conformation. Although the helical form would not accumulate in the presence of membranes, it provides a convenient assembly for understanding an intermediate step in pore formation.

The asymmetric subunit shape accommodates domains 1, 2, and 4 approximately in the positions shown in Figure 4a. The changes from the soluble monomer structure are dramatic, most notably the 45° rotation of domain 4 and the loss of much of the domain 3 density. In the presence of membrane, the toxin would bind to cholesterol and oligomerize on the bilayer surface. In the absence of membrane and at high toxin concentration this process occurs spontaneously in solution. The upward movement of domain 4 accompanying oligomerization pushes domain 3 toward the inside of the forming ring (Figure 4b). Since the α-helical region of domain 3 adjacent to domain 2 has been implicated in membrane insertion (Palmer et al., 1996; Shepard et al., 1998), its release from the monomeric configuration prepares the way for this region to refold and enter the membrane. In the absence of membrane, this intermediate conformation has been trapped, and domain 3 occupies a range of positions away from domain 2, causing its density to be smeared out and lost from the images. Consistent with this idea, the domain 2/3 interface is not well packed in the monomer crystal structure (Rossjohn et al., 1997).

The Pore Conformation

The cryo-EM views of the liposomes show the membranes studded with pore structures located mainly outside the bilayer (Figure 5). Thin extensions project downward and contact the membrane. The 3D reconstruction of the membrane-bound pore (Figure 5d) revealed a third distinct conformation of the pneumolysin subunit, in which the domain 3 density is recovered and packed against domain 2 (Figure 6a). The model is compatible with the extension of the α-helical region into the β hairpin structure proposed by Shepard et al. (1998). This could enter the membrane alongside the base of domain 4. The 30-residue stretch of domain 3 proposed to enter the membrane could form a β hairpin spanning 45 Å. However, the distance from the ends of this region to the membrane surface in our pore model is roughly 40 Å. It may be that this region only partially inserts into the membrane or that the movement toward the membrane involves extension of additional parts of domain 3.

The pore reconstruction does not show a large opening in the membrane, although the bilayer structure shows fluctuations in density with spacings of 60–80 Å (Figure 5d). These features could correspond to nonbilayer configurations such as inverted hexagonal lipid phases (Seddon, 1990). The lowest density region of the membrane is just outside the protein subunit. Negative-stain EM images of face views of the rings on membranes show a very dark region inside the pore (e.g., Bhakdi et al., 1985; Morgan et al., 1994), apparently revealing a large opening in the membrane. However, the height of the ring above the membrane means that
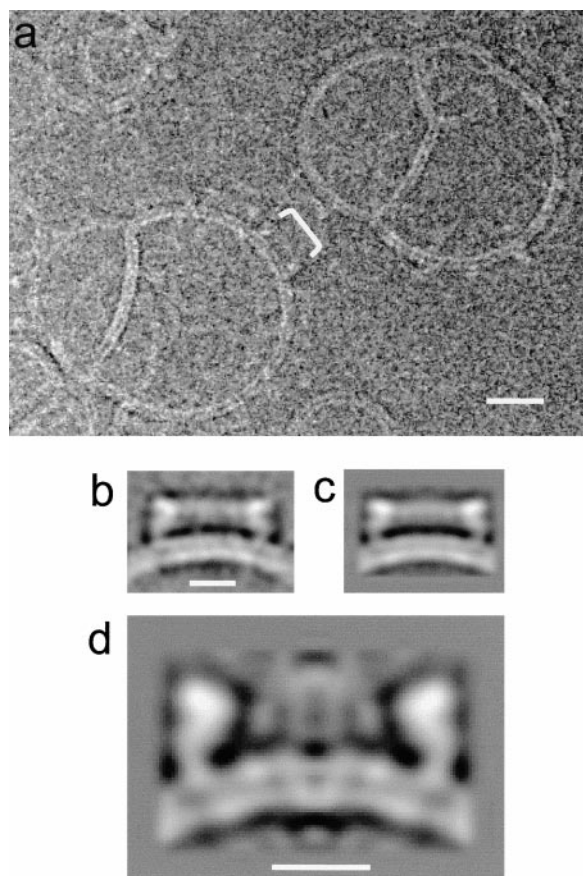
Figure 5. Cryo-EM of Liposomes with Pneumolysin Pores

(a) Raw image of liposomes with bound pores. The edges of the pores give spike-like projections. One pore side view is marked by a white bracket. Indistinct end views of rings are faintly visible on the larger liposomes.

(b) Average of 26 side views after alignment and classification, showing the pore structure above the membrane surface.

(c) Reprojection of a 3D reconstruction of the pore, showing good agreement with the averaged side view.

(d) Slice through the 3D reconstruction of the pore. The subunit shape and its stalk-like connection to the membrane are evident. The membrane bilayer appears to be continuous but has density fluctuations. The lowest density region of the membrane is just outside the pore subunits.

Scale bars: (a), 300 Å; (b and c), 100 Å; (d), 100 Å.

it could collect stain to give this appearance even if the membrane below it were continuous. Clearly, permeability studies indicate a major disruption to the membrane by the pores (Buckingham and Duncan, 1983). The cryo-EM side views may not all be complete rings, which could confuse the appearance of the membrane. Further work is needed to determine the state of the membrane within the pore and the precise extent to which the toxin protein penetrates the membrane.

Mechanism of Oligomerization and Pore Formation

The soluble monomer, free oligomer, and pore conformations of the pneumolysin subunit are shown in Figure 7, along with models of the oligomeric forms. The most conserved region in the cholesterol-binding toxin sequence is the Trp-rich loop (residues ECTGLAWEWWR)
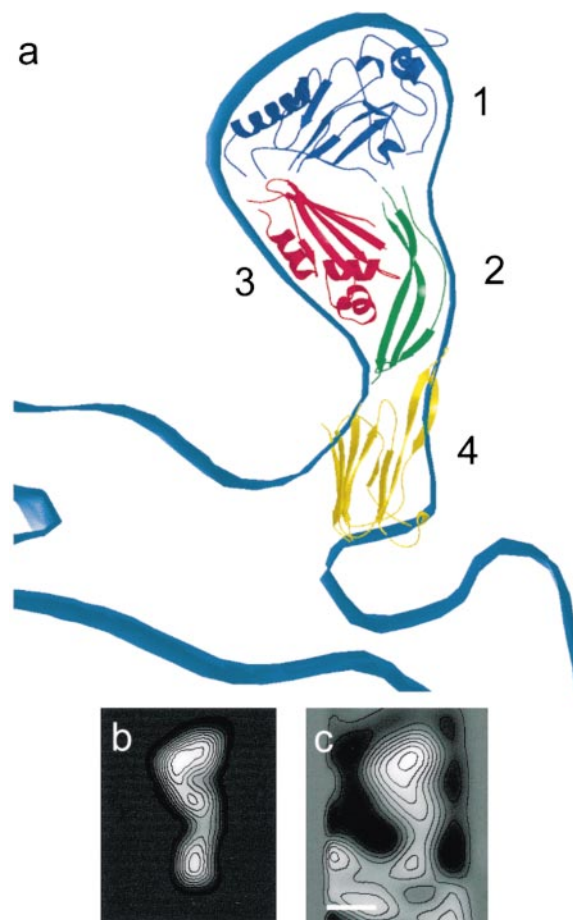

Figure 6. Fit of the Four Domains to the Pore Subunit Density

(a) The right-hand side of the pore section is shown with the domains fitted into the density. Almost the whole pneumolysin molecule can be accounted for by density outside the membrane. The domains are numbered and colored as in Figure 4.

(b) 33 Å resolution projection of the model created by fitting the four domains to the subunit density after deleting the helical region (residues 189–218) of domain 3.

(c) Section of the subunit density showing a reasonable correspondence with the model in (b).

Scale bar for (b) and (c), 30 Å.

at the base of domain 4. Mutations or chemical modifications in this region reduce or abolish membrane binding and/or pore formation (Hill et al., 1994; Jones et al., 1996), or modulate apparent pore size and conductance (Korchev et al., 1998). The position of domain 4 in the pore form suggests that the Trp-rich loop enters the membrane, consistent with fluorescence and circular dichroism spectroscopy results (Nakamura et al., 1995, 1998). Binding to the membrane may elicit the extension of the loop to the dagger structure as previously proposed (Rossjohn et al., 1997). Our results indicate that oligomerization occurs by a two-step mechanism. First, the domain 3 helical region (residues 189–218; 158–187 in pneumolysin) is released from its location inside the monomer by the extrusion of domain 3. Then this region can extend to contact the membrane as the domains repack.

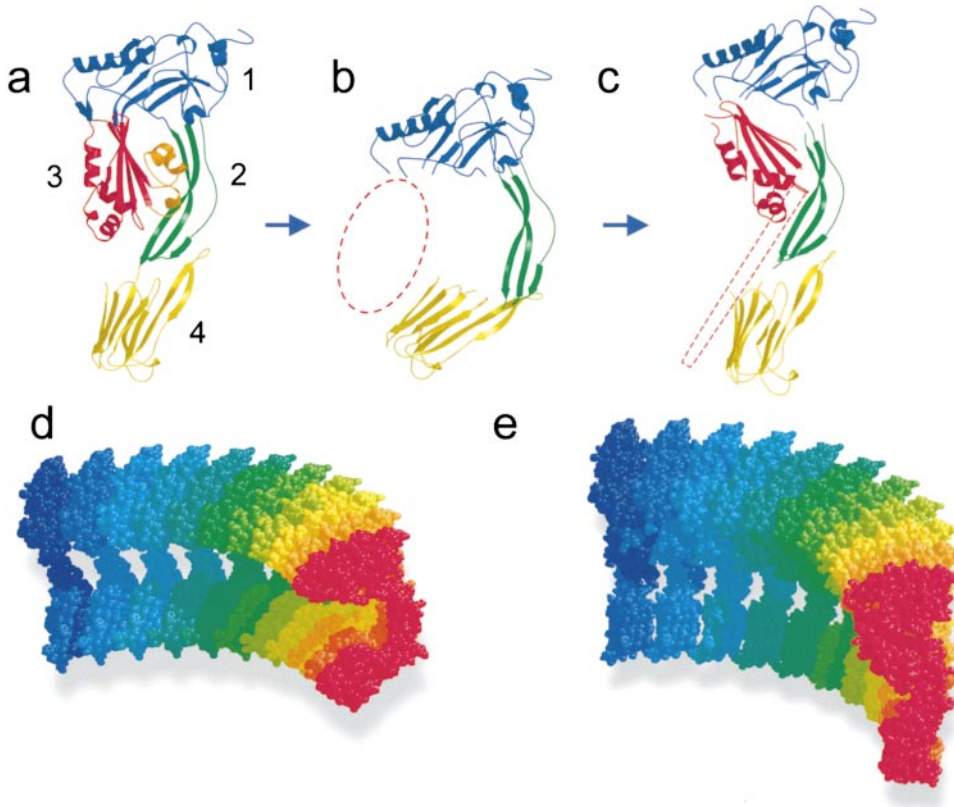Dimerization is thought to be the rate-limiting step in

Figure 7. Model of Pore Formation

Domain positions are shown in the soluble monomer (a), compared to the isolated ring (subunit conformation fitted to the helical structure [b]) and to the membrane-bound oligomer (c). The domains are numbered and colored as in Figure 4. The position of domain 3 in (b) is schematically indicated by the dashed outline, as is the hairpin loop in (c). Partial oligomer models are shown in space-filling format for free (d) and bound (e) rings.

pore formation (Palmer et al., 1995). Additional subunits would undergo the domain 4 rotation and domain 3 expulsion in solution or on the membrane, but only the growing membrane-bound oligomers would be able to insert the domain 3 loop into the membrane. There is clear evidence that incomplete oligomers (arcs) can form conducting pores (Palmer et al., 1998). The existence of arc-shaped pores makes it unlikely that the inserted regions join up to form the wall of a transmembrane channel, since this would have an edge bound by free membrane. Although this type of structure was proposed by Palmer et al (1998), it does not explain what would stop the surface pressure of the bilayer from causing the free edge to fill in an arc-shaped hole. Local perturbation of the bilayer structure may be a physically more reasonable idea. For example, the Trp-rich antibiotic peptide gramicidin, which also interacts with cholesterol (de Kruijff, 1990) may induce membrane bilayers to form inverted hexagonal phases (Killian et al., 1996). For this type of bilayer disruption, it may not be necessary for the protein to completely cross the membrane. A wedge-shaped insertion would be sufficient to destabilize the bilayer structure, by driving a set of spikes into the planar bilayer and changing the proportion of area available for lipid headgroups and tails. Formation of nonlamellar structures such as inverted hexagonal lipid phases would lead to the breakdown of the permeability barrier.

Comparison with Other Pore-Forming Toxins

Other toxins oligomerize to form pores. The protective antigen (PA) of *Bacillus anthracis* (Petosa et al., 1997) and α-hemolysin of *Staphylococcus aureus* (Song et al., 1996) form heptameric structures. For α-hemolysin, the pore is formed by a 14-stranded transmembrane β barrel formed from β hairpins contributed by each subunit in the oligomer. PA has been crystallized in both monomeric and prepore oligomeric forms (Petosa et al., 1997). Apart from the proteolytic removal of the top of the first PA domain to facilitate oligomerization, there were no large differences in structure between the two forms. It is thought that in PA the membrane-inserting hairpin is formed from a polypeptide loop disordered in the monomer. In the case of the α-hemolysin family, both a monomer (LukF, Olson et al., 1999) and a pore structure (Song et al., 1996) have been determined to atomic resolution. In the monomer structure, the pore-forming region is folded back onto the main body of the toxin, extending a β sheet. In both cases, the main conformational change between monomer and oligomeric pore form is in the loop that inserts, or is thought to insert, into the membrane, with no major changes in the rest of the structure.

The transition undergone by cholesterol-binding toxins, as revealed by spectroscopic analyses of perfringolysin (Shepard et al., 1998) and the present study of oligomeric states of pneumolysin by cryo-EM, describes

an entirely different mechanism of pore formation. Here, the proposed refolding and insertion of a pore-forming sequence from α helix to β sheet (Shepard et al., 1998) is enabled by a two-stage conformational change involving massive domain rotations and the release of this sequence from its initial location buried inside the protein. Furthermore, each pneumolysin subunit may be anchored to the membrane by both domains 3 and 4. Neither region appears to cross the bilayer, and the membrane may instead be destabilized by partial insertions promoting nonbilayer lipid phases.

Experimental Procedures

Sample Preparation

Pneumolysin was expressed and purified as described previously (Gilbert et al., 1998). For oligomerization, it was incubated at 3–7 mg/ml either in 125 mM PBS (8 mM Na_2HPO_4, 1.5 mM KH_2PO_4, 2.5 mM KCl, 125 mM NaCl [pH 7.48]) made with 99.9% D_2O, or with 100% H_2O. The yield of helical oligomers was higher in D_2O (Gilbert et al., 1998). Typically the toxin was incubated for 1 hr at 37°C. The yield of helical oligomers could be further increased by pelletting, resuspending, and reincubating the samples. Unfortunately, this tended to promote aggregation of the toxin oligomers.

Liposomes were prepared as follows. A mixture of 10:10:1 hen egg white phosphatidylcholine:cholesterol:dicetyl phosphate in 1:1 (v/v) chloroform:methanol was dried under a stream of nitrogen. The dried lipids were dissolved in buffer (50 mM NaH_2PO_4, 200 mM NaCl) containing 3% w/v Mega-8 (octanoyl-N-methylglucamide, Sigma) to a final lipid concentration of 2 mM, and the solution was vortexed. The suspension was then sonicated at 45°C for 1 hr in a DECON FS200 frequency sweep water-bath sonicator (DECON Ltd, Hove, Sussex, UK). The preparation was then filtered through a 0.2 μm acrodisc sterile filter and dialyzed into the same buffer lacking Mega-8 in 2000× excess for 72 hr with at least four changes.

Monomeric pneumolysin was added to the liposomes at a molar ratio of 1:100 pneumolysin:cholesterol. The mixture was incubated at room temperature for 30 min and then vitrified for cryo-EM.

Electron Microscopy, Image Processing, and 3D Reconstruction

Samples of pneumolysin oligomers or pore-containing liposomes were vitrified after briefly floating the grids on a water droplet to wash out salt. Images were collected on a JEOL 2010 HC TEM (JEOL Ltd, Tokyo, Japan) operating at 200 kV, with an Oxford Instruments cryo-transfer stage (Oxford Instruments Ltd, Oxford, U.K.).

Negatives were scanned on a LeafScan 45 CCD scanner (Ilford Ltd, Cheshire, UK) at 6.67 Å/pixel. Processing was done using MRC (Crowther et al., 1996), Imagic (van Heel et al., 1996), or Suprim (Schroeter and Bretaudiere, 1996) software. The images of helical oligomers were sorted into groups on the basis of their power spectra. This revealed two classes of helices, with a 100 Å and a 135 Å repeat. The ones with the larger repeat were better ordered, and these were used for further processing. The helices were straightened using a Suprim procedure kindly provided by Dr. B. Carragher. Because the helical pitch was variable, the straightened helices were divided up into individual pitch repeats, with some overlap to allow for subsequent alignment, using the strategy described in Jiménez et al. (1999). The averaged repeat obtained by Fourier filtering the layer lines of the best helical diffraction pattern was used as a starting model. This was cross-correlated with each straightened fiber in both up and down orientations, in order to determine the polarity or to exclude fibers without clear polarity. One hundred twenty-five repeats were excised using the centers determined in the correlation, averaged, and iteratively aligned. Classification was used to select a set of consistent repeats from untilted fibers, and the resulting averaged image of the pitch repeat (containing 33 repeats) was used to generate the helical reconstruction by back projection. The alignment, classification, and reconstruction steps were iterated. The number of subunits per turn was known to be 40–50 from previous work on the ring form (Morgan et al., 1995). A

reconstruction with 41 subunits per turn gave a good match to the input projection and to the diffraction pattern of a straightened helix (Figure 2). A range of subunit repeats gave similar results, and the precise value of the subunit repeat does not affect our interpretation, because it does not alter the density cross section that determines the layout of domains in the plane of the subunit. The diffraction pattern of the reprojected helical density showed layer line intensities to about 25 Å resolution. It should be noted that the handedness of the helix is not determined by this method and is arbitrary. However, this does not affect the observed subunit shape at this resolution.

Ninety-seven tangential views of pores on the surfaces of liposomes were selected, aligned, and classified into groups of similar views. The best class contained 26 views. Using the class average, in which the ring diameter fitted ~33 subunits, a 3D reconstruction was made by filtered back projection of the average in steps of 360°/33°. Fourier ring correlation indicated a resolution of ~33 Å at a cutoff of 0.5.

Atomic Structure Fitting

The four perfringolysin domains were fitted as rigid bodies into the helical and pore density maps by manual fitting in O (Jones et al., 1991), using CCP4 programs (CCP4, 1994) for data conversion. It is clear from EM views and the map dimensions that the plane of the molecules is vertical and that the major movements are in that plane. Therefore, the in-plane domain rotations could be determined by this relatively simple approach. No attempt was made to adjust the hinge regions or alter subunit conformations, as such procedures were not justified by the accuracy of the maps. Using SPIDER (Frank et al., 1996), the fitted coordinates were converted to electron density, which was then filtered to low resolution in order to generate electron density maps of the fits for comparison with EM data. Oligomer models were created from the fitted monomers by applying the appropriate rotations without further adjustment. The resulting subunit interfaces fitted reasonably well together if the appropriate rotation angle (number of subunits per ring) was chosen.

The molecular structure figures were prepared with BOBSCRIPT and rendered with RASTER3D (Kraulis, 1991; Merritt and Murphy, 1994; Esnouf, 1997).

References

Alexander, J.E., Berry, A.M., Paton, J.C., Rubins, J.B., Andrew, P.W., and Mitchell, T.J. (1998). Amino acid changes affecting the activity of pneumolysin alter the behaviour of pneumococci in pneumonia. Microb. Pathog. *24*, 167–174.

Alonso de Velasco, E., Verheuil, A.F.M., Verhoef, J., and Snippe, H. (1995). *Streptococcus pneumoniae*: virulence factors, pathogenesis, and vaccines. Microbiol. Rev. *59*, 591–603.

Bayley, H. (1997). Toxin structure: part of a hole? Curr. Biol. *7*, R763–R767.

Berry, A.M., Yother, J., Briles, D.E., Hansman, D., and Paton, J.C. (1989). Reduced virulence of a defined pneumolysin-negative mutant of *Streptococcus pneumoniae*. Infect. Immun. *57*, 2037–2042.

Bhakdi, S., Tranum-Jensen, J., and Sziegoleit, A. (1985). Mechanism of membrane damage by streptolysin O. Infect. Immun. *47*, 52–60.

Buckingham, L., and Duncan, J.L. (1983). Approximate dimensions of membrane lesions produced by streptolsyin S and streptolysin O. Biochim. Biophys. Acta *279*, 115–122.

CCP4 (Collaborative Computational Project) Program Suite. (1994). The CCP4 suite: programs for protein crystallography. Acta Crystallogr. D *50*, 750–763.

Crowther, R.A., Henderson, R., and Smith, J.M. (1996). MRC image processing programs. J. Struct. Biol. *116*, 9–16.

de Kruijff, B. (1990). Cholesterol as a target for toxins. Biosci. Rep. *10*, 127–130.

Esnouf, R.M. (1997). An extensively modified version of MOLSCRIPT that includes greatly enhanced coloring capabilities. J. Mol. Graph. *15*, 132–134.

Frank, J., Radermacher, M., Penczek, P., Zhu, J., Li, Y., Ladjadj, M., and Leith, A. (1996). SPIDER and WEB: processing and visualization of images in 3D electron microscopy and related fields. J. Struct. Biol. *119*, 190–199.

Gilbert, R.J.C., Rossjohn, J., Parker, M.W., Tweten, R.K., Morgan, P.J., Mitchell, T.J., Errington, N., Rowe, A.J., Andrew, P.W., and Byron, O. (1998). Self-interaction of pneumolysin, the pore forming protein toxin of *Streptococcus pneumoniae*. J. Mol. Biol. *284*, 1223–1237.

Grindstaff, K.K., Yeaman, C., Anandasabapathy, N., Hsu, S.C., Boulan, E.R., Scheller, R.H., and Nelson, W.J. (1998). Sec6/8 complex is recruited to cell-cell contacts and specifies transport vesicle delivery to the basal-lateral membrane in epithelial cells. Cell *93*, 731–740.

Harris, R.W.. Sims, P.J., and Tweten, R.K. (1991). Kinetic aspects of the aggregation of *Clostridium perfringens* θ-toxin on erythrocyte membranes. J. Biol. Chem. *266*, 6936–6941.

Hill, J., Andrew, P.W., and Mitchell, T.J. (1994). Amino acids in pneumolysin important for hemolytic activity identified by random mutagenesis. Infect. Immun. *62*, 757–758.

Jiménez, J.L., Guijarro, J.I., Orlova, E., Zurdo, J., Dobson, C.M., Sunde, M., and Saibil, H.R. (1999). Cryo-electron microscopy structure of an SH3 amyloid fibril and model of the molecular packing. EMBO J. *118*, 815–821.

Jones, T.A., Zhou, J.-Y., Cowan, S.W., and Kjeldgaard, M. (1991). Improved methods for building models in electron density maps and the location of errors in these models. Acta Crystallogr. *A47*, 110–119.

Jones, S., Preiter, K., and Portnoy, D.A. (1996). Conversion of an extracellular cytolysin into a phagosome-specific lysin which supports the growth of an intracellular pathogen. Mol. Microbiol. *21*, 1219–1225.

Killian, J.A., Salemink, I., De Planque, M.R.R., Lindblom, G., Koeppe, R.E., and Greathouse, D.V. (1996). Induction of non-bilayer structures in diacylphosphatidylcholine model membranes by transmembrane α-helical peptides: importance of hydrophobic mismatch and proposed role of tryptophans. Biochemistry *35*, 1037–1045.

Korchev, Y.E., Bashford, C.L., Pederzolli, C., Pasternak, C.A., Morgan, P.J., Andrew, P.W., and Mitchell, T.J. (1998). A conserved tryptophan in pneumolysin is a determinant of the characteristics of channels formed by pneumolysin in cells and planar lipid bilayers. Biochem. J. *329*, 571–577.

Kraulis, P.J. (1991). MOLSCRIPT—a program to produce both detailed and schematic plots of protein structures. J. Appl. Crystallogr. *24*, 946–950.

Merritt, E.A., and Murphy, M.E.P. (1994). RASTER3D version-2.0—a program for photorealistic molecular graphics. Acta Crystallogr. *D 50*, 869–873.

Mitchell, T.J., Andrew, P.W., Saunders, F.K., Smith, A.N., and Boulnois, G.J. (1991). Complement activation and antibody binding by pneumolysin via a region of the toxin homologous to a human acute-phase protein. Mol. Microbiol. *5*, 1883–1888.

Morgan, P.J., Hyman, S.C., Byron, O., Andrew, P.W., Mitchell, T.J., and Rowe, A.J. (1994). Modeling the bacterial protein toxin, pneumolysin, in its monomeric and oligomeric form. J. Biol. Chem. *269*, 25315–25320.

Morgan, P.J., Hyman, S.C., Rowe, A.J., Mitchell, T.J., Andrew, P.W., and Saibil, H.R. (1995). Subunit organisation and symmetry of pore-forming oligomeric pneumolysin. FEBS Lett. *371*, 77–80.

Morgan, P.J., Andrew, P.W., and Mitchell, T.J. (1996). Thiol-activated cytolysins. Rev. Med. Microbiol. *7*, 221–229.

Nakamura, M., Sekino, N., Iwamoto, M., and Ohno-Iwashita, Y. (1995). Interaction of theta-toxin (perfringolysin-O), a cholesterol-binding cytolysin, with liposomal membranes: change in the aromatic sidechains upon binding and insertion. Biochemistry *34*, 6513–6520.

Nakamura, M., Sekino-Suzuki, N., Mitsui, K., and Ohno-Iwashita, Y. (1998). Contribution of tryptophan residues to the structural changes in perfringolysin O during interaction with liposomal membranes. J. Biochem. *123*, 1145–1155.

Olofsson, A., Hebert, H., and Thelestam, M. (1993). The projection structure of perfringolysin O (*Clostridium perfringens* θ-toxin). FEBS Lett. *319*, 125–127.

Olson, R., Nariya, H., Yokota, K., Kamio, Y., and Gouaux, E. (1999). Crystal structure of staphylococcal LukF delineates conformational changes accompanying formation of a transmembrane channel. Nat. Struct. Biol. *6*, 134–140.

Palmer, M., Valeva, A., Kehoe, M., and Bhakdi, S. (1995). Kinetics of streptolysin O self-assembly. Eur. J. Biochem. *231*, 388–395.

Palmer, M., Saweljew, P., Vulicevic, I., Valeva, A., Kehoe, M., and Bhakdi, S. (1996). Membrane-penetrating domain of streptolysin O identified by cysteine scanning mutagenesis. J. Biol. Chem. *271*, 26664–26667.

Palmer, M., Harris, J.R., Freytag, C., Kehoe, M., Tranum-Jensen, J., and Bhakdi, S. (1998). Assembly mechanism of the oligomeric streptolysin O pore: the early membrane lesion is lined by a free edge of the lipid membrane and is extended gradually during oligomerization. EMBO J. *17*, 1598–1605.

Petosa, C., Collier, R.J., Klimpel, K.R., Leppla, S.H., and Liddington, R.C. (1997). Crystal structure of the anthrax toxin protective antigen. Nature *385*, 833–838.

Rossjohn, J., Feil, S.C., McKinstry, W.J., Tweten, R.K., and Parker, M.W. (1997). Structure of a cholesterol-binding, thiol-activated cytolysin and a model of its membrane form. Cell *89*, 685–692.

Rossjohn, J., Gilbert, R.J.C., Crane, D., Morgan, P.J., Mitchell, T.J., Rowe, A.J., Andrew, P.W., Paton, J.C., Tweten, R.K., and Parker, M.W. (1998). The molecular mechanism of pneumolysin, a virulence factor from *Streptococcus pneumoniae*. J. Mol. Biol. *284*, 449–461.

Schroeter, J.P., and Bretaudiere, J.P. (1996). SUPRIM—easily modified image-processing software. J. Struct. Biol. *116*, 131–137.

Seddon, J.M. (1990). Structure of the inverted hexagonal (H_{II}) phase, and non-lamellar phase transitions of lipids. Biochim. Biophys. Acta *1031*, 1–69.

Sekiya, K., Satoh, R., Danbara, H., and Futaesaku, Y. (1993). A ring-shaped structure with a crown formed by streptolysin O on the erythrocyte membrane. J. Bacteriol. *175*, 5953–5961.

Shepard, L.A., Heuck, A.P., Hamman, B.D., Rossjohn, J., Parker, M.W., Ryan, K.R., Johnson, A.E., and Tweten, R.K. (1998). Identification of a membrane-spanning domain of the thiol-activated pore-forming toxin *Clostridium perfringens* perfringolysin: an α-helical to β-sheet transition identified by fluorescence spectroscopy. Biochemistry *37*, 14563–14574.

Song, L.Z., Hobaugh, M.R., Shustak, C., Cheley, S., Bayley, H., and Gouaux, J.E. (1996). Structure of staphylococcal α-hemolysin, a heptameric transmembrane pore. Science *274*, 1859–1866.

Tweten, R.K. (1995). Pore-forming toxins in gram-positive bacteria. In Virulence Mechanisms of Bacterial Pathogens, J.A. Roth, C.A. Bolin, K.A. Brogden, C. Minion, and M.J. Wannemuehler, eds. (Washington D.C.: American Society for Microbiology), pp. 207–229.

van Heel, M., Harauz, G., Orlova, E.V., Schmidt, R., and Schatz, M. (1996). A new generation of the IMAGIC image processing system. J. Struct. Biol. *116*, 17–24.

Watson, K.C., Rose, T.P., and Kerr, E.J.C. (1972). Some factors influencing the effect of cholesterol on streptolysin O activity. J. Clin. Path. *25*, 885–891.